Hindawi
Advances in Civil Engineering
Volume 2018, Article ID 2757542, 14 pages
https://doi.org/10.1155/2018/2757542

Research Article

Effect of Deficiencies in the Tunnel Crown Thickness on Pressure Tunnels with Posttensioned Concrete Linings

Gan Qin, Shengrong Cao, and Fan Yang

State Key Laboratory of Water Resources and Hydropower Engineering Science, Wuhan University, Wuhan 430072, China

Correspondence should be addressed to Shengrong Cao; shrcao@whu.edu.cn

Received 11 October 2017; Accepted 20 May 2018; Published 11 July 2018

Academic Editor: Giovanni Garcea

This paper investigates the effect of deficiencies in the tunnel crown thickness on pressure tunnels with the posttensioned concrete lining. Based on the lining parameters of the Yellow River Crossing Tunnel, the modeling approach of the posttensioned concrete lining is introduced in detail and a three-dimensional finite element model is established. The three-dimensional finite element model is validated by experimental results from the full-scale model experiment of the Yellow River Crossing Tunnel. Special attention is given to the changes in the deformation, radial displacement, and circumferential stress of the posttensioned concrete lining with gradual decreases in the tunnel crown thickness. The calculation results show that the influence scopes of deficiencies in the tunnel crown thickness are mainly concentrated in the crown and its adjacent parts. The posttensioned concrete lining can still maintain a satisfactory stress state when deficiencies in the tunnel crown thickness exist, and undesirable stress levels may be caused only when the tunnel crown thickness decreases below a certain threshold. Furthermore, cracks are most likely to occur at the external and internal surfaces of the crown and at the internal surface of the crown's adjacent parts, which is useful for taking measurements regarding the lining tightness and stability.

1. Introduction

Antiseepage is an important requirement for tunnels subjected to high internal water pressure. The posttensioned concrete lining (PTCL) is considered to be a suitable solution to improve the water impermeability of such tunnels. For the PTCL, the anchor cable is tensioned and anchored in the anchorage slot. After the completion of tensioning and anchoring, lining concrete can be held in a fully compressed state by introducing prestress, ensuring stability and watertightness [1, 2]. The details of the PTCL are illustrated in Figure 1. The first pressure tunnel with the PTCL was constructed at Piastra-Andonno in Italy in 1974, and many such tunnels have been constructed since then, such as the water conveyance tunnel of Geheyan Hydropower Station, the water conveyance tunnel of the Grimsel project in Switzerland, and the desilting tunnel of Xiaolangdi Dam [3].

Despite the specified requirements and supervisions in quality control during the construction of the concrete lining, construction errors may exist due to careless construction [4]. Among the various construction errors that may occur, deficiency in the tunnel crown thickness is a common problem that exists in the concrete lining. For example, Yang and Fu [5] reported the results of a nondestructive detection test of a curved tunnel, which showed that the tunnel crown thickness was approximately 30–40 cm, considerably less than the design value of 50 cm. In addition, Zhu et al. [6] used nondestructive testing methods to evaluate the construction quality of the Wuzhuling Tunnel in China. The results showed that the tunnel crown was the main location where the thickness was less than the design value. Bian et al. [7] also found that the minimum thickness of concrete in the crown of a bifurcation tunnel was only 20 cm according to drill tests, considerably less than the design value of 60 cm.

Many negative consequences result from deficiencies in the tunnel crown thickness. For example, Bian et al. [7] reported a wide range of cracking that occurred in the concrete lining at the crown of a bifurcation tunnel at the Huizhou Pumped Storage Power Station and found that the deficiency in the tunnel crown thickness was the primary

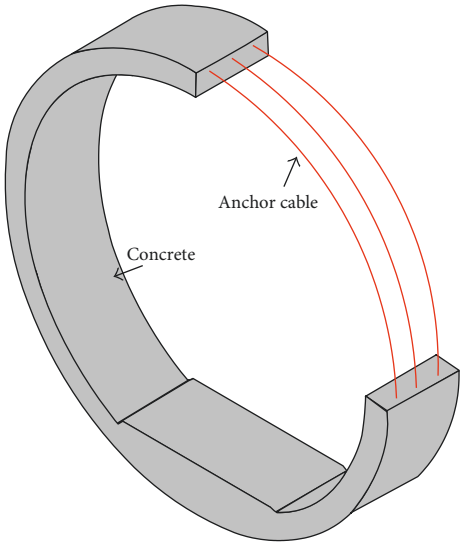

Figure 1: Details of the PTCL.

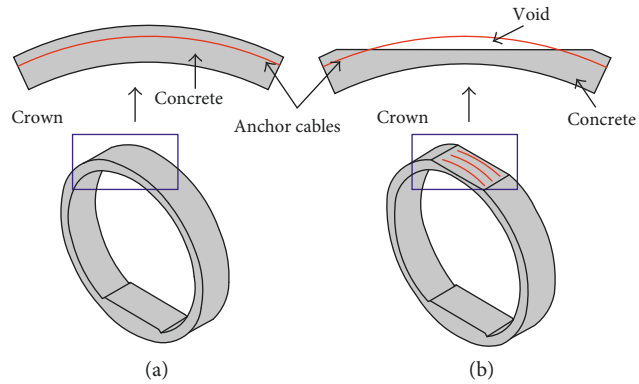

Figure 2: PTCL: (a) the tunnel crown thickness is equal to the design value and (b) the tunnel crown thickness is less than the design value.

factor causing the lining cracking. Voids may remain between the rock surface and concrete lining when the thickness of the tunnel crown is insufficient. The voids can induce surface corrosion of tunnel appurtenances, deterioration of the concrete lining with an associated reduced load-carrying capacity, and even failure of the concrete lining [8, 9]. In addition, the final cross section of the concrete lining will be different from the design requirements because of deficiencies in the tunnel crown thickness. Barpi and Peila [10] and Son and Cording [11] have noted that an irregular cross section of the concrete lining would induce concentrated stress in the concrete lining, which could in turn result in cracking and even local collapses.

The above research suggests that deficiencies in the tunnel crown thickness can cause widespread damage to the concrete lining, ranging from concrete cracking to local collapses. However, all of the above achievements have focused on reinforced concrete linings. Few studies have focused on the PTCL, for which deficiencies in the tunnel crown thickness may generate more complex problems. For the PTCL with insufficient tunnel crown thickness, a void may form and the anchor cable at the crown may hang in the void, as shown in Figure 2. Because there is no concrete to support the partial anchor cable located at the crown, the shape of the anchor cable will differ from the intended design once it is tensioned. Moreover, the stress level in the anchor cable is always very high [12]. For example, the design tension stress of the anchor cable is 1,395 MPa for the Yellow River Crossing Tunnel. The unintended curvature of the anchor cable and the high stress in the anchor cable will induce stress redistribution in the PTCL and may cause an undesirable stress level in the PTCL. Therefore, there is a clear and justified need to evaluate the effect of deficiencies in the tunnel crown thickness on the PTCL.

The paper represents its kind analysis for the potential influence of deficiencies in the tunnel crown thickness on pressure tunnels with the PTCL for the first time. The Yellow River Crossing Tunnel in the Middle Route of the South-to-North Water Diversion Project is adopted as a reference case. Based on the soil and lining parameters of the Yellow River Crossing Tunnel, the modeling approach of the PTCL is introduced in detail and a three-dimensional finite element model is established. To evaluate the effect of deficiencies in the tunnel crown thickness on the PTCL during the construction phase and operation phase, two working conditions are analyzed: the completed cable tensioning condition (CCTC) and water in the tunnel with the design water pressure condition (DWPC). Changes in the deformation, radial displacement, and circumferential stress of the PTCL with gradual decreases in the tunnel crown thickness are investigated. Furthermore, the locations at which cracks in the PTCL are most likely to occur are also identified.

2. Basic Information about the Yellow River Crossing Tunnel

The Yellow River Crossing Tunnel, located in Zhengzhou city, China, is a key component of the Middle Route of the South-to-North Water Diversion Project. The Yellow River Crossing Tunnel passes through soft soil and was constructed by the shield tunnelling method. The precast segments are assembled to withstand the soil pressure and the external water pressure during excavation. The internal water pressure in the centre of the tunnel is more than 0.5 MPa during the operation phase. If the internal water pressure is borne only by the segmental lining, the segmental joints will be a large opening, resulting in water seepage. Therefore, the PTCL is needed as the secondary lining to withstand the high internal water pressure. When the segmental lining has already borne the external pressure and achieved stability, the PTCL begins to be poured. The bottom of the PTCL is directly poured on the segmental lining, and the others are separated from the segmental lining by the membrane. The membrane can play a role in waterproofing and drainage [13].

The PTCL of the Yellow River Crossing Tunnel has an inner diameter of 7 m, an outer diameter of 7.9 m, and a thickness of 0.45 m. An anchor cable has a design tension stress of 1,395 MPa and includes 12 steel strands. Each steel strand contains 7 high-strength and low-relaxation steel

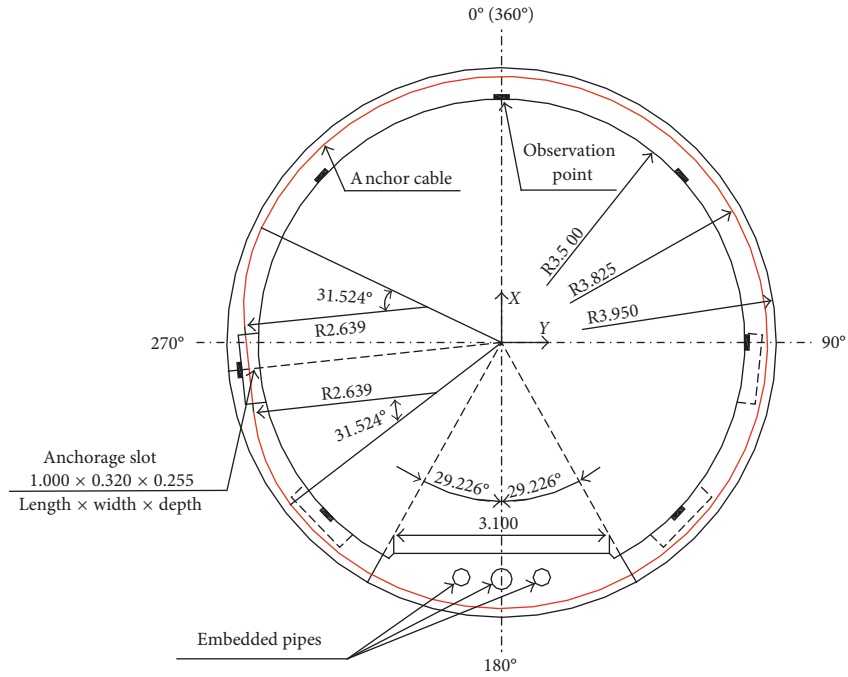

Figure 3: Cross section of the PTCL (unit: m).

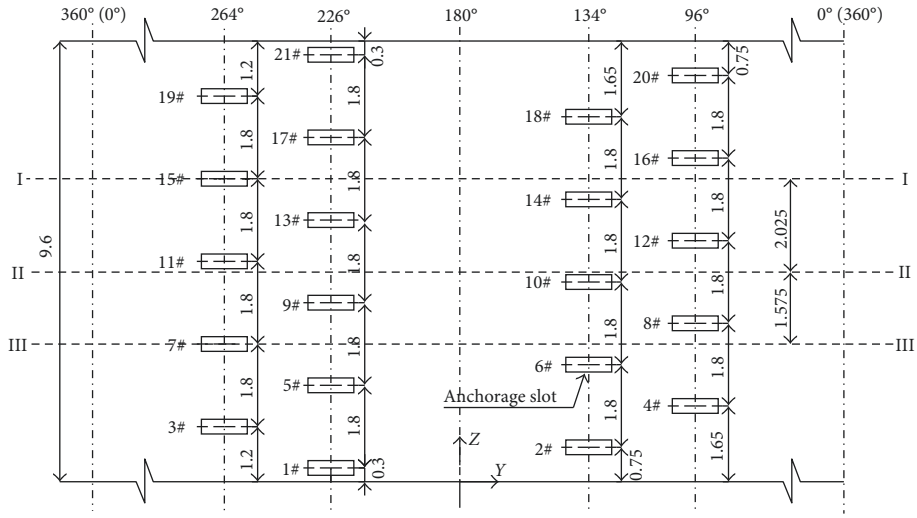

Figure 4: Layout of the internal surface of the PTCL (unit: m).

wires. The centre lines of the anchorage slots are located at angles of 96°, 134°, 226°, and 264°. The distance between adjacent anchorage slots is 0.45 m along the axial direction. The cross section of the PTCL is shown in Figure 3. The layout of the internal surface of the PTCL is shown in Figure 4.

3. Numerical Model

3.1. Model Details. The numerical model is established by taking a 9.6 m length along the axial direction of the tunnel. The numerical model is restrained in the horizontal direction at the lateral boundaries and is restrained in both the vertical and horizontal directions at the bottom boundary. The upper boundary has no constraints. The lateral and bottom boundaries of the discretization are placed at positions with a sufficient distance, namely, 4 times the tunnel diameter. The upper boundary is placed directly on the ground surface with a sufficient distance, which is approximately 5 times the tunnel diameter. The soil strata, where the Yellow River Crossing Tunnel is situated, comprised medium sand. Small amounts of clay strata are present below the tunnel. The strata distribution is shown in Figure 5.

A typical finite element mesh of the Yellow River Crossing Tunnel is shown in Figure 6. Eight-noded solid elements are employed to simulate the soil strata, concrete, and membrane [14]. Two-noded link elements are employed

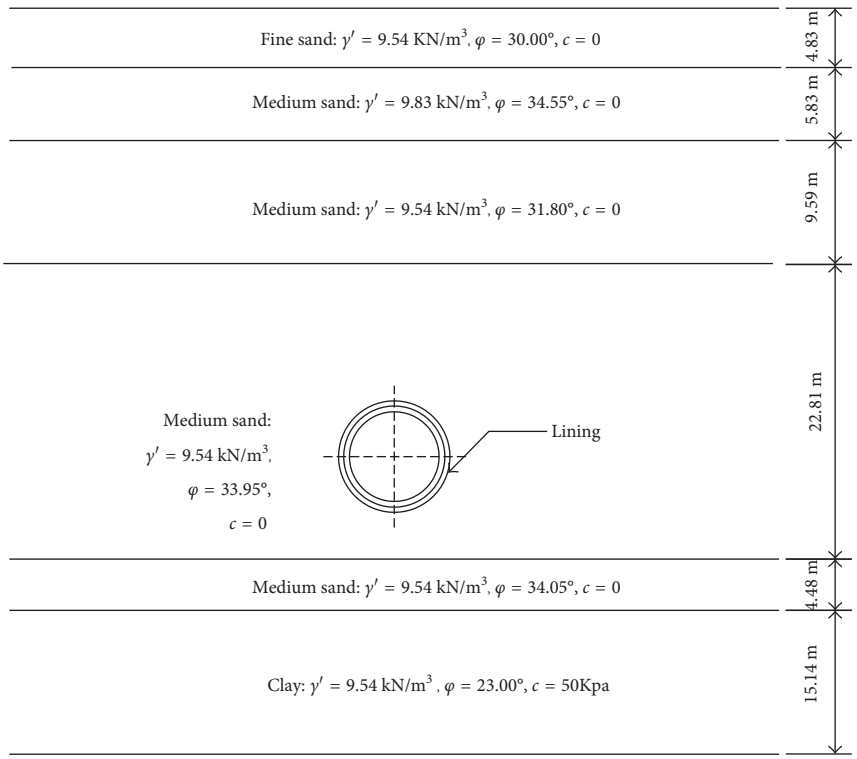

Figure 5: Distribution of the soil strata. γ' = effective unit weight; φ = friction angle; c = cohesion; E = elastic modulus of soil (40 MPa); μ = Poisson's ratio (0.3).

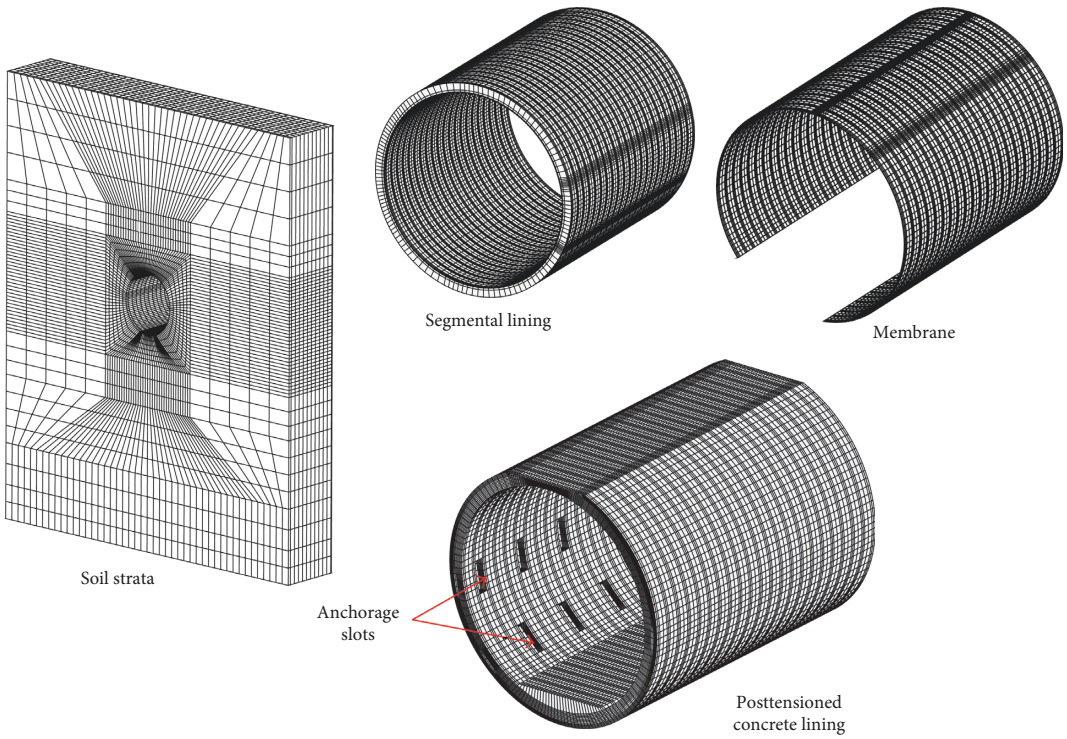

Figure 6: Finite element models.

to simulate the anchor cable and reinforcing bar in the PTCL. A perfect bond between the link elements and solid elements is assumed. The concrete and membrane are assumed to be elastic materials. The material properties for the Yellow River Crossing Tunnel are listed in Table 1. The soil strata are approximated as elastoplastic following the

Table 1: Material properties.

Part	Material	Elasticity modulus, E (MPa)	Poisson's ratio, ν	Unit weight, γ (KN·m^{-3})
PTCL	C40 concrete	3.25×10^4	0.167	24.5
Segmental lining	C50 concrete	3.45×10^4	0.167	25
Membrane	Composite material	1.5	0.3	—
Anchor cable	Steel	1.95×10^5	0.3	78.5
Reinforcing bar	Steel	2.0×10^5	0.3	80

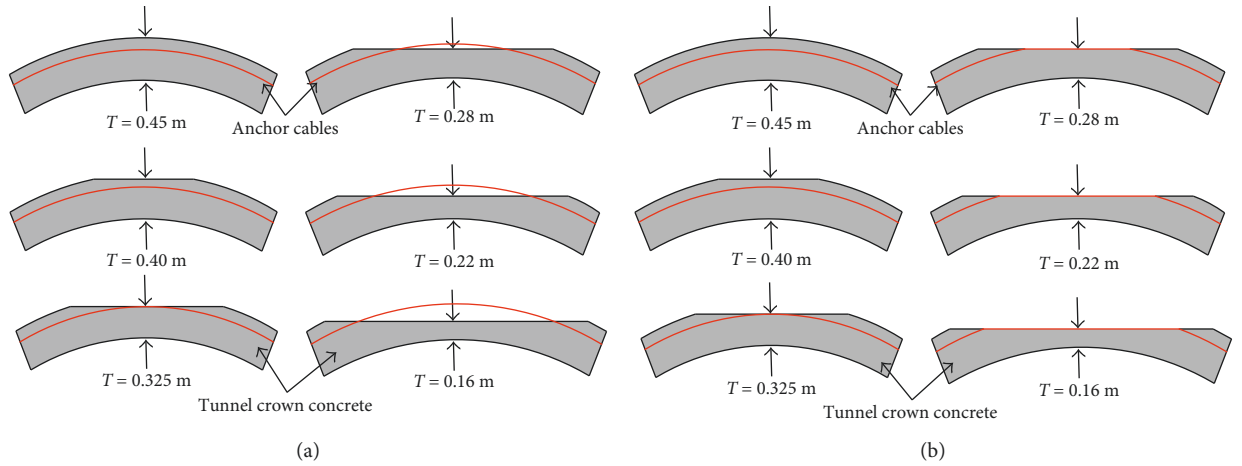

Figure 7: Six cases considering different concrete thicknesses in the tunnel crown: (a) before tensioning of the anchor cable and (b) after tensioning of the anchor cable.

Drucker–Prager failure criterion. The strength parameters of the soil strata are listed in Figure 5. The numerical model contains 284,520 elements and 295,485 nodes.

The interfaces between the internal surfaces of the membrane and the external surfaces of the PTCL and interfaces between the soil excavation boundary and the external surfaces of the segmental lining are simulated by contact elements. The contact behaviour in the radial direction is simulated as a hard contact transmitting compressive stresses but cannot transmit radial tensile stresses [15, 16]. The Coulomb friction model is used to limit the tangential tractions. A value of 0.3 is selected as the friction coefficient, and the penalty method is adopted as the contact algorithm [17, 18].

Six simplified cross sections of the PTCL with insufficient tunnel crown thickness are introduced, as shown in Figure 7. T represents the thickness of the tunnel crown, and six cases of T have been selected in this paper: 0.45, 0.40, 0.325, 0.28, 0.22, and 0.16 m. The thickness of the tunnel crown is assumed to be the same along the axial direction of the lining. The anchor cables can be supported by concrete when $T = 0.45$, 0.40, and 0.325 m, as shown in Figure 7(a). However, when $T = 0.28$, 0.22, and 0.16 m, the anchor cables located at the crown will hang in the void. Because there is no concrete to support the partial anchor cables located at the crown, the partial anchor cables located at the crown will be straight lines once they are tensioned, as shown in Figure 7(b).

3.2. Calculation of the Prestress. When the anchor cable tension is completed, the prestresses (σ_1) are not constant due to friction between the anchor cable and the duct. The shapes of the anchor cables at the crown are curved when T is equal to or greater than 0.325 m, and they are straight lines when T is less than 0.325 m. Therefore, the calculation of σ_1 considering the frictional losses should be divided into two cases. When T is equal to or greater than 0.325 m as shown in Figure 8(a), σ_1 can be expressed as

$$\sigma_1 = \begin{cases} \sigma_{\text{con}} e^{-(\kappa r_c + \mu)\varphi}, & 0^\circ \le \varphi < 180^\circ \\ \sigma_{\text{con}} e^{-(\kappa r_c + \mu)(360^\circ - \varphi)}, & 180^\circ \le \varphi \le 360^\circ, \end{cases} \tag{1}$$

where μ is the friction coefficient between the anchor cable and duct, k is the wobble friction coefficient per meter of the anchor cable, r_c is the curvature radius of the anchor cable, σ_{con} is the design tension stress of the anchor cable, and φ is the cumulative angle change between the tensioning position and calculation section.

When T is less than 0.325 m as shown in Figure 8(b), σ_1 can be calculated by

$$\sigma_1 = \begin{cases} \sigma_{\text{con}} e^{-(\kappa r_c + \mu)\varphi}, & 0^\circ \le \varphi \le \varphi_A \\ \sigma_{\text{con}} e^{-(\kappa r_c + \mu)\varphi_A} e^{(-\mu\beta)}, & \varphi_A < \varphi \le \varphi_B \\ \sigma_{\text{con}} e^{-(\kappa r_c + \mu)\varphi_A} e^{(-2\mu\beta)} e^{-(\kappa r_c + \mu)(\varphi - \varphi_B)}, & \varphi_B < \varphi \le \phi \\ \sigma_{\text{con}} e^{-(\kappa r_c + \mu)(360^\circ - \varphi)}, & \phi < \varphi \le 360^\circ, \end{cases} \tag{2}$$

where φ_A is the cumulative angle change between the tensioning position and location A, φ_B is the cumulative angle change between the tensioning position and location B, β is

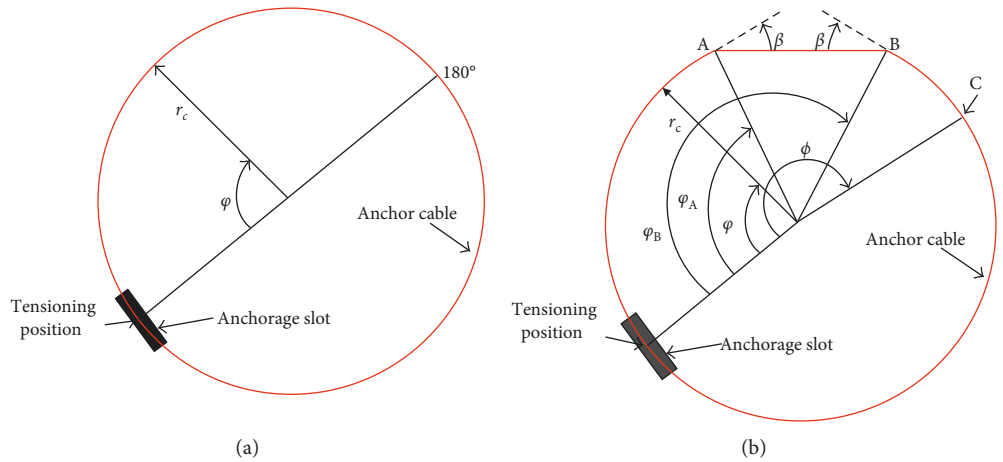

FIGURE 8: Calculation of the prestress: (a) T is equal to or greater than 0.325 m and (b) T is less than 0.325 m.

the angle between the tangent of the anchor cable at location A and the horizontal line, and ϕ is the angle which can be calculated by

$$e^{-(\kappa r_c+\mu)(360^\circ-\phi)} = e^{(-2\mu\beta)} e^{-(\kappa r_c+\mu)\varphi_A} e^{-(\kappa r_c+\mu)(\phi-\varphi_B)}. \quad (3)$$

Prestress losses of the anchor cables are inevitable, and prestress losses after tensioning of the anchor cable considered in the numerical model mainly include σ_{l1} caused by anchorage deformation and anchor cable retraction, σ_{l2} caused by stress relaxation of the anchor cable, and σ_{l3} caused by concrete shrinkage and creep [19]. σ_{l1}, σ_{l2}, and σ_{l3} can be calculated following the formulas recommended by the Code for Design of Concrete Structure [20]. σ_{l1} can be expressed as follows:

$$\sigma_{l1} = \begin{cases} \sigma_{con} e^{-(\kappa r_c+\mu)\varphi} \left[1 - e^{-2(\kappa r_c+\mu)(\varphi_0-\varphi)}\right], & 0 \le \varphi \le \varphi_0 \\ 0, & \varphi > \varphi_0, \end{cases} \quad (4)$$

where φ_0 is the influence range of antifriction resistance which can be calculated by

$$\varphi_0 = \frac{1}{(\mu + kr_c)} \ln\left[1 - \sqrt{\frac{aE}{\sigma_{con}} \cdot \frac{(\mu + kr_c)}{1000 r_c}}\right]^{-1}, \quad (5)$$

where a is the anchorage deformation and reinforcement retraction value and E is the elastic modulus of the anchor cable. σ_{l2} and σ_{l3} can be expressed as follows:

$$\sigma_{l2} = 0.20\left[\frac{\sigma_{con}}{f_{ptk}} - 0.575\right]\sigma_{con}, \quad (6)$$

$$\sigma_{l3} = \frac{55 + 300\left(\sigma_{pc}/f_{cu}\right)}{1 + 15\rho}, \quad (7)$$

where f_{ptk} is the characteristic value of anchor cable strength, σ_{pc} is the normal compressive stress of concrete at the point of resultant force for the anchor cable, f_{cu} is the cube compressive strength of concrete when applying prestress, and ρ is the reinforcement ratio of the concrete compression zone.

Finally, the effective prestresses σ_{pe} can be expressed by

$$\sigma_{pe} = \sigma_1 - \sigma_{l1} - \sigma_{l2} - \sigma_{l3}. \quad (8)$$

The effective prestresses are converted into the temperature loads, and the temperature loads are applied to the anchor cable elements [21]. The temperature loads can be expressed by

$$t = -\frac{\sigma_{pe}}{E\alpha}, \quad (9)$$

where t is the temperature load applied to the anchor cable elements and α is the expansion coefficient of the anchor cable.

3.3. Load Combinations of Calculation Stages. According to the construction process and the operating conditions of the Yellow River Crossing Tunnel, two main calculation stages are considered. The first stage is the CCTC, in which the PTCL is poured and the anchor cable tension is completed. The second stage is the DWPC, in which the internal water pressure is applied on the PTCL. The load combinations of each working condition are shown in Table 2.

The external water pressure in the horizontal line of the tunnel centre is 0.323 MPa. The internal water pressure in the tunnel centre is 0.517 MPa. Separate calculations of water pressure and earth pressure can be used when the tunnel is covered by sandy soil [22]. So, the external water pressure is directly applied on the segmental lining and the effective unit weight of the soil strata is adopted.

3.4. Validation of the Numerical Model. The numerical model is validated by experimental data from the full-scale model experiment of the Yellow River Crossing Tunnel [23, 24]. As shown in Figure 4, three sections (sections I–III) are observed in the full-scale model experiment. Each section has seven observation points, and the centre lines of the observation points are located at angles of 0°, 45°, 90°, 135°, 225°, 270°, and 315°, as shown in Figure 3. Because the tunnel

Table 2: Load combinations of the working conditions.

Working conditions	Gravity	Soil pressure	External water pressure	Effective prestress	Internal water pressure
CCTC	√	√	√	√	—
DWPC	√	√	√	√	√

Table 3: Average circumferential stresses of the observation sections (unit: MPa).

	Section I		Section II		Section III	
	CCTC	DWPC	CCTC	DWPC	CCTC	DWPC
Experimental results	−7.74	−4.19	−7.36	−2.98	−7.14	−4.21
Numerical results	−7.00	−3.31	−7.12	−2.88	−6.62	−3.27

crown thickness of the experimental model is 0.45 m, we can only compare the numerical results with the experimental results for the case of $T = 0.45$ m.

The average circumferential stresses of the observation points under the CCTC and DWPC are summarized in Table 3. Under the CCTC, the calculated average circumferential stresses of the sections I, II, and III are −7.00, −7.12, and −6.62 MPa, respectively, which are 9.5%, 3.3%, and 7.3% lower than the corresponding experimental values. Under the DWPC, the calculated average circumferential stresses of the sections I, II, and III are −3.31, −2.88, and −3.27 MPa, respectively, which are 21%, 3.5%, and 22.3% lower than the corresponding experimental values. There are some errors between experimental results and numerical results, which may be caused by the concrete vibrator or other interference factors that affected the strain gauges during the experiment. However, the comparison still indicates a general agreement between the numerical results and experimental results.

4. Results and Discussion

A series of finite element analyses have been performed to examine the effect of deficiencies in the tunnel crown thickness on the PTCL. Section II is selected as the typical section, and the numerical results of section II are shown in Figures 9–14.

4.1. Deformation of the PTCL. The calculated deformations of the PTCL under the CCTC and DWPC are shown in Figures 9 and 10, respectively, which also reveal the PTCL's radial displacement at the crown. Positive displacement represents direction toward outward of the PTCL, and negative displacement denotes direction toward inward of the PTCL.

According to Figure 9(a), when T is equal to the design value (0.45 m), the PTCL deforms inward at the crown. As shown in Figures 9(b) and 9(c), gradual decreases in the crown thickness can induce an increase in inward movements at the crown. This behaviour occurs because the crown concrete of the PTCL is thin, which reduces the stiffness of the crown concrete. During the tensioning process, the crown concrete is squeezed by the anchor cables located at the crown, which results in an increase in inward movements.

In contrast, a different trend occurs when T is less than 0.325 m. According to Figures 9(d)–9(f), further gradual decreases in the crown thickness can induce an increase in outward movements at the crown and the crown concrete will have a discernible bulge toward outward of the PTCL. This behaviour occurs because the anchor cables hang in the voids and cannot restrain the deformation of the crown concrete. During the tensioning process, the crown concrete is squeezed by the anchor cables on both sides of the crown, which results in a discernible bulge toward outward of the PTCL. A similar phenomenon can also be observed under the DWPC, as shown in Figure 10.

4.2. Radial Displacement of the PTCL. The calculated radial displacement of the PTCL under the CCTC and DWPC in six cases is shown in Figure 11, where θ is the angle measured clockwise from the vertical plane. Figure 11 illustrates that the influence scopes of deficiencies in the tunnel crown thickness on the radial displacement are mainly concentrated in the crown and its adjacent parts. In other words, there are only slight changes in the radial displacement in other parts of the PTCL with variations in the crown thickness.

The maximum radial displacement of the PTCL is located at the crown ($\theta = 0^\circ$), and the distribution of the radial displacement remains fairly constant when T is equal to or greater than 0.28 m. As shown in Figure 11(a), the radial displacement at the crown for $T = 0.28$ m is −6.87 mm. This radial displacement is 9.9% higher than that at $T = 0.45$ m. As shown in Figure 11(b), the radial displacement at the crown for $T = 0.28$ m is −4.98 mm, which is 5.1% lower than that at $T = 0.45$ m. The above comparison indicates that a deficiency in the tunnel crown thickness has only a slight effect on the values and distributions of the PTCL's radial displacement when T is equal to or greater than 0.28 m.

When T is less than 0.28 m, the distribution of the radial displacement changes, and the maximum radial displacement of the PTCL transfers from the crown ($\theta = 0^\circ$) to its adjacent parts. As shown in Figure 11(a), the radial displacement at the crown for $T = 0.16$ m is −4.92 mm, which is 23.1% lower than that at $T = 0.45$ m. As shown in Figure 11(b), the radial displacement at the crown for $T = 0.16$ m is −0.24 mm, which is 95.4% lower than that at $T = 0.45$ m. The crown radial displacement values change

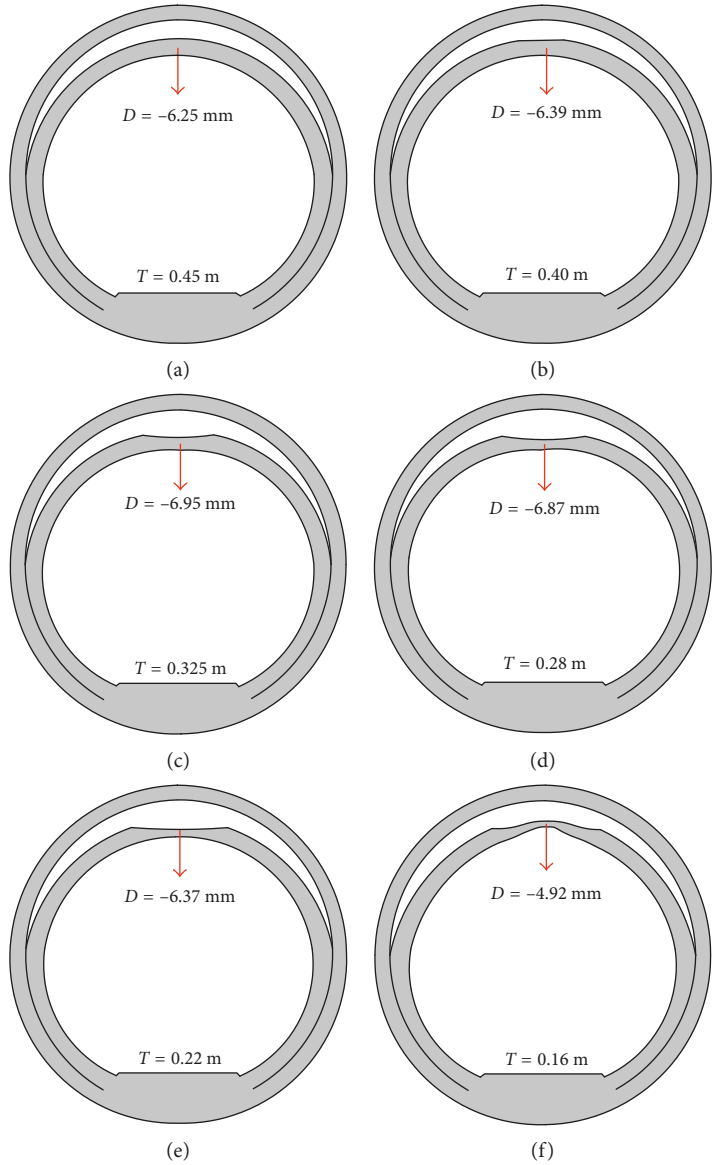

Figure 9: Deformations of the PTCL under the CCTC: (a) $T = 0.45$ m, (b) $T = 0.40$ m, (c) $T = 0.325$ m, (d) $T = 0.28$ m, (e) $T = 0.22$ m, and (f) $T = 0.16$ m.

considerably when T is less than 0.28 m, which illustrates that the existence of deficiencies in the tunnel crown thickness leads to a substantial increase in the deformation at the crown. As we know, failure is probable to occur at large deformation parts of the concrete lining, and the large deformation at the crown could in turn result in cracking and even local collapses.

4.3. Circumferential Stresses of the PTCL. The circumferential stresses of the internal surface and external surface of the PTCL are shown in Figures 12 and 13 in a polar system of coordinates, respectively. Positive stress represents tensile stress, and negative stress denotes compressive stress.

According to Figures 12(a)–12(c), the circumferential stresses of the internal surface range from 0 to −10 MPa in the majority of the PTCL. Considering that the tensile strength of C40 concrete is 2.45 MPa, deficiencies in the tunnel crown thickness will not lead to lining cracking at the internal surface in any of the three cases. In other words, the internal surface of the PTCL can still maintain a satisfactory stress state when T is equal to or greater than 0.325 m.

In contrast, when T is less than 0.325 m, the internal surface of the PTCL crown will become the compressive stress concentrated zone. The maximum compressive stress will increase considerably with further gradual decreases in the crown thickness. As shown in Figure 12(e), the maximum compressive stress of the PTCL's internal surface is −14.36 MPa under the CCTC, which is 143.4% higher than that at $T = 0.45$ m. According to Figure 12(f), the maximum compressive stress of the PTCL's internal

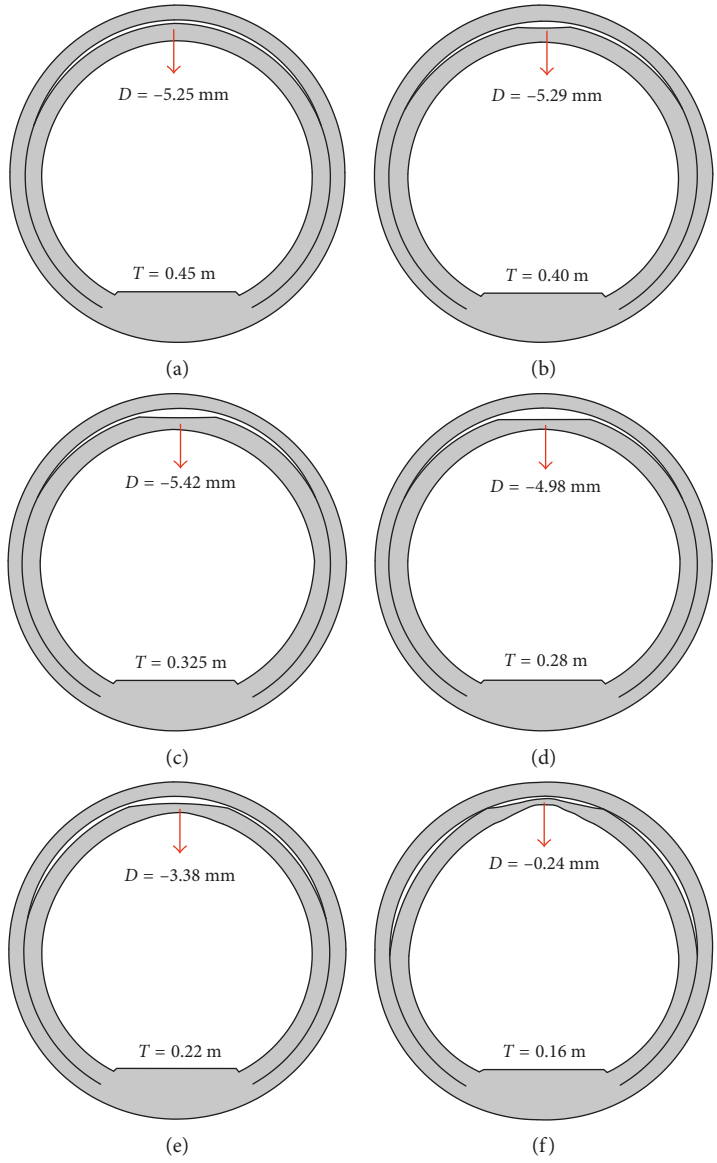

Figure 10: Deformations of the PTCL under the DWPC: (a) $T = 0.45$ m, (b) $T = 0.40$ m, (c) $T = 0.325$ m, (d) $T = 0.28$ m, (e) $T = 0.22$ m, and (f) $T = 0.16$ m.

surface is −24.53 MPa under the CCTC, which is 315.8% higher than that at $T = 0.45$ m. Considering that the compressive strength of C40 concrete is −27 MPa, concrete at the crown may be crushed during the tensioning process if the crown thickness decreases further.

The results in Figures 12(e) and 12(f) also show that partial parts of the PTCL's internal surface are subjected to tensile stresses under the DWPC. The tensile parts are mainly located at the upper semicircle of the PTCL. With further gradual decreases in the crown thickness, the tensile parts will become larger and the maximum tension stress will incrementally increase. As shown in Figures 12(e) and 12(f), the maximum tension stress of the internal surface under the DWPC increases from 3.38 MPa for $T = 0.22$ m to 10.31 MPa for $T = 0.16$ m, representing a 205% increase. In these two cases, the tension stresses have already exceeded the tensile strength of the C40 concrete and may lead to cracking or even failure of the PTCL.

According to Figures 13(a)–13(c), the circumferential stresses of the external surface range from 0 MPa to −12.56 MPa in the majority of the PTCL. Considering the tensile strength and compressive strength of C40 concrete, deficiencies in the tunnel crown thickness will not lead to lining cracking at the external surface in any of the three cases. In other words, the external surface of PTCL can still maintain a satisfactory stress state when T is equal to or greater than 0.325 m.

In contrast, when T is less than 0.325 m, partial parts of the PTCL's external surface will be subjected to tensile stresses under the DWPC. As shown in Figure 13(d), the tensile parts are mainly located at the tunnel crown,

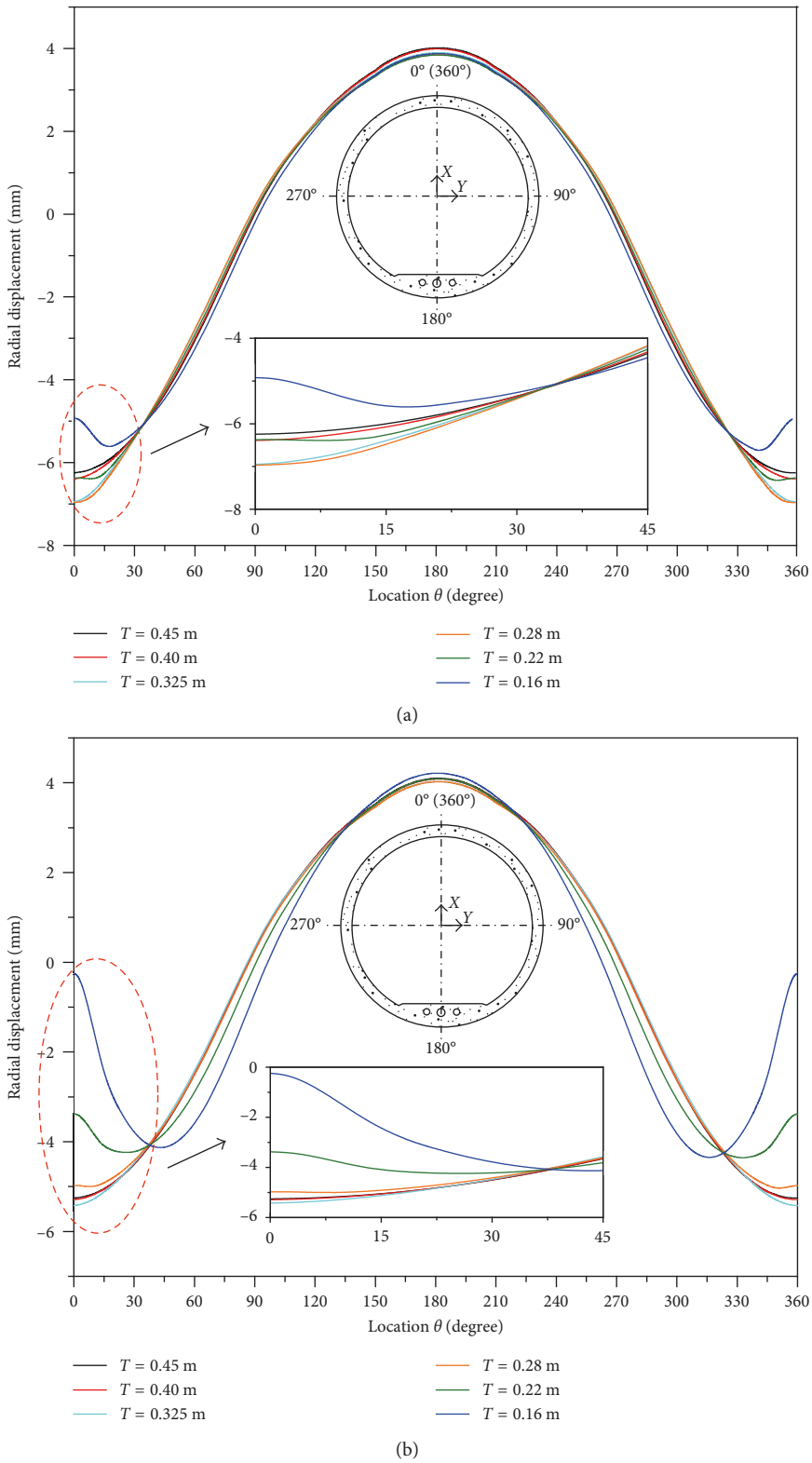

Figure 11: Radial displacement of the PTCL: (a) CCTC and (b) DWPC.

and the maximum tensile stress of the PTCL's external surface is 0.37 MPa. With further gradual decreases in the crown thickness, the tensile parts will become larger and the maximum tension stress will incrementally increase. As shown in Figure 13(e), the maximum tension stress of the PTCL's external surface under the DWPC increases from

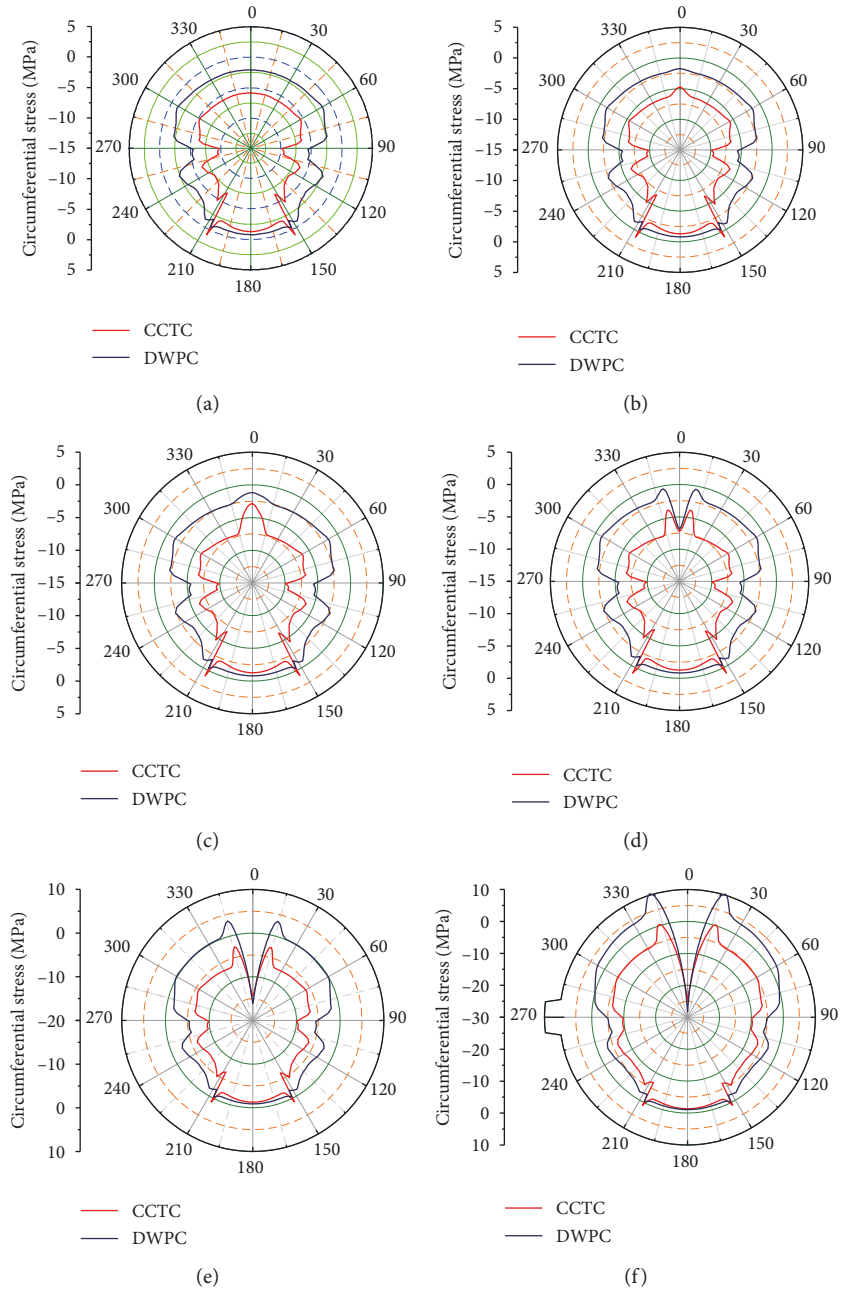

Figure 12: Circumferential stresses of the PTCL's internal surface: (a) $T = 0.45$ m, (b) $T = 0.40$ m, (c) $T = 0.325$ m, (d) $T = 0.28$ m, (e) $T = 0.22$ m, and (f) $T = 0.16$ m.

0.37 MPa for $T = 0.28$ m to 7.9 MPa for $T = 0.22$ m. As shown in Figure 13(f), the maximum tension stress of the PTCL's external surface under the DWPC is 19.1 MPa, which is 141.8% higher than that at $T = 0.22$ m. The tension stresses are 3 to 8 times the tensile strength of the C40 concrete in these two cases, which will lead to cracking or even failure of the PTCL.

4.4. Damaged Locations of the PTCL. The above findings imply that the PTCL will be subjected to tensile stresses under the DWPC if the deficiencies in the tunnel crown thickness exceed a certain threshold. Figure 14 shows the locations (the red zones) where the tension stresses have already exceeded the tensile strength of the PTCL to visualize the parts where cracks are likely to occur in the PTCL. For such cases as $T = 0.22$ m and $T = 0.16$ m, the crown's adjacent parts deform inward, and the internal surface of the crown's adjacent parts will be under tension. Therefore, cracks may occur at the internal surface of the crown's adjacent parts. At the same time, the crown concrete has a discernible bulge toward outward of the PTCL as shown in Figures 9 and 10, and

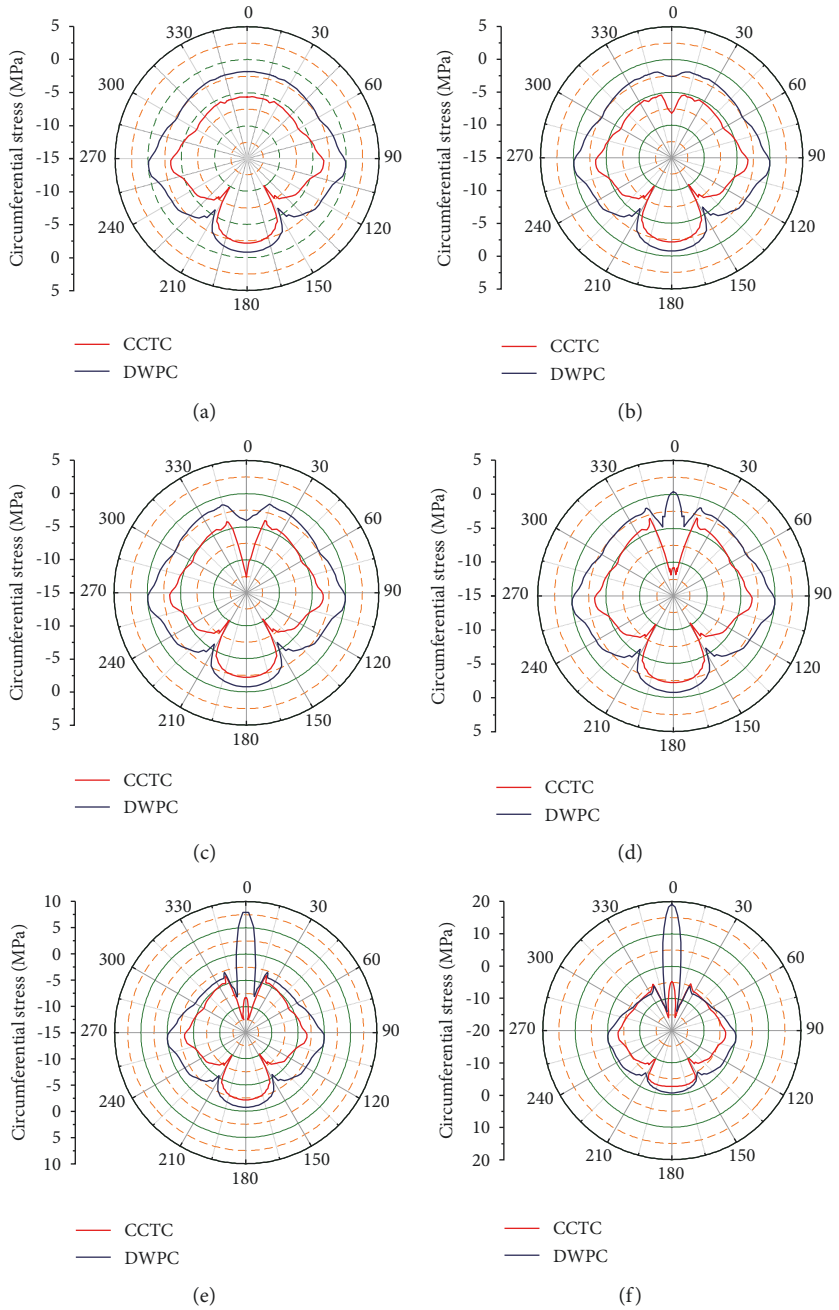

Figure 13: Circumferential stresses of the PTCL's external surface: (a) $T = 0.45$ m, (b) $T = 0.40$ m, (c) $T = 0.325$ m, (d) $T = 0.28$ m, (e) $T = 0.22$ m, and (f) $T = 0.16$ m.

the external surface of the crown will be under tension. Thus, cracks at the external surface of the crown may also be expected.

5. Conclusions

This paper investigates the effect of deficiencies in the tunnel crown thickness on the PTCL. The Yellow River Crossing Tunnel is adopted as a reference case, and numerical analyses are performed using a three-dimensional finite element model. The three-dimensional finite element model is validated by experimental data from the full-scale model experiment of the Yellow River Crossing Tunnel. The possible damage and corresponding locations are discussed. The following conclusions are drawn from the results with the conditions and assumptions given in this study:

(1) The influence scopes of deficiencies in the tunnel crown thickness are mainly concentrated in the tunnel crown and its adjacent parts. There are only small changes in the deformation, radial displacement, and circumferential stress in the other parts

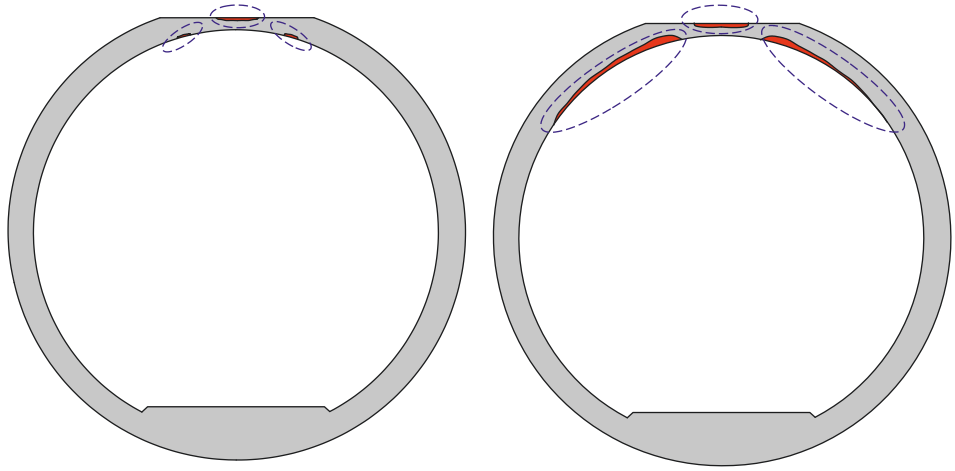

Figure 14: Locations where the tension stresses have already exceeded the tensile strength of the PTCL under the DWPC: (a) $T = 0.22$ m and (b) $T = 0.16$ m.

of the PTCL considering variations in the tunnel crown thickness.

(2) The PTCL can still maintain a satisfactory stress state with the existence of deficiencies in the tunnel crown thickness. Undesirable stress levels may occur only when the tunnel crown thickness decreases below a certain threshold.

(3) Compressive stress concentration of the tunnel crown's internal surface is notable, and the internal surface of the tunnel crown concrete may be crushed under the CCTC. Because the cracks form during the tensioning process, such crushing may be readily detected.

(4) Cracks at the external surface of the crown and internal surface of the crown's adjacent parts may be expected under the DWPC. Because the cracks form during the filling of the tunnel with water, they may not be readily detected until serious damage to the lining has been produced, generally in the form of severe cracking, leaking, or even failure.

Conflicts of Interest

The authors declare that there are no conflicts of interest regarding the publication of this paper.

Acknowledgments

This work is supported by the Hubei Province Natural Science Foundation of China (no. 2017CFB667), the State Key Laboratory of Hydrology-Water Resources and Hydraulic Engineering Foundation (no. 2015494711), and the National Natural Science Foundation of China (no. 51079107). Additionally, the provision of the original data by the Changjiang Institute of Survey, Planning, Design and Research is gratefully acknowledged.

References

[1] U. H. Grunicke and M. Ristić, "Pre-stressed tunnel lining-pushing traditional concepts to new frontiers," *Geomechanics and Tunnelling*, vol. 5, no. 5, pp. 503–516, 2012.

[2] K. Nishikawa, "Development of a prestressed and precast concrete segmental lining," *Tunnelling and Underground Space Technology*, vol. 18, no. 2-3, pp. 243–251, 2003.

[3] J. F. Kang and Y. M. Hu, "Techniques and performance of post-prestressed tunnel liner," *Practice Periodical on Structural Design and Construction*, vol. 10, no. 2, pp. 102–108, 2005.

[4] Y. Yuan, Y. Bai, and J. Liu, "Assessment service state of tunnel structure," *Tunnelling and Underground Space Technology*, vol. 27, no. 1, pp. 72–85, 2012.

[5] J. S. Yang and J. Y. Fu, "Investigation and rehabilitation of lining imperfections and cracks in an operating railway tunnel," in *Proceedings of Shotcrete for Underground Support XII*, pp. 1–10, Whistler, BC, USA, September 2015.

[6] C. Zhu, F. Lei, and J. Dong, "Structure detection and evaluation of highway tunnels based on geological radar detection technology," in *Proceedings of Challenges and Advances in Sustainable Transportation Systems, ASCE*, pp. 547–554, Beijing, China, May 2014.

[7] K. Bian, J. Liu, M. Xiao, and Z. Liu, "Cause investigation and verification of lining cracking of bifurcation tunnel at Huizhou Pumped Storage Power Station," *Tunnelling and Underground Space Technology*, vol. 54, pp. 123–134, 2016.

[8] M. A. Meguid and H. K. Dang, "The effect of erosion voids on existing tunnel linings," *Tunnelling and Underground Space Technology*, vol. 24, no. 3, pp. 278–286, 2009.

[9] Z. Wang, L. Wang, L. Li, and J. Wang, "Failure mechanism of tunnel lining joints and bolts with uneven longitudinal ground settlement," *Tunnelling and Underground Space Technology*, vol. 40, pp. 300–308, 2014.

[10] F. Barpi and D. Peila, "Influence of the tunnel shape on shotcrete lining stresses," *Computer-Aided Civil and Infrastructure Engineering*, vol. 27, no. 4, pp. 260–275, 2012.

[11] M. Son and E. J. Cording, "Ground-liner interaction in rock tunneling," *Tunnelling and Underground Space Technology*, vol. 22, no. 1, pp. 1–9, 2007.

[12] F. M. Li, Y. S. Yuan, and C. Q. Li, "Corrosion propagation of prestressing steel strands in concrete subject to chloride attack," *Construction and Building Materials*, vol. 25, no. 10, pp. 3878–3885, 2011.
[13] F. Yang, S. Cao, and G. Qin, "Performance of the prestressed composite lining of a tunnel: case study of the Yellow River Crossing Tunnel," *International Journal of Civil Engineering*, vol. 16, no. 2, pp. 229–241, 2017.
[14] M. Yousaf, Z. A. Siddiqi, M. B. Sharif, and A. U. Qazi, "Force- and displacement-controlled non-linear FE analyses of RC beam with partial steel bonded length," *International Journal of Civil Engineering*, vol. 15, no. 4, pp. 499–513, 2016.
[15] J. Wang, H. Huang, X. Xie, and A. Bobet, "Void-induced liner deformation and stress redistribution," *Tunnelling and Underground Space Technology*, vol. 40, pp. 263–276, 2014.
[16] J. Kim, J. C. Yoon, and B. S. Kang, "Finite element analysis and modeling of structure with bolted joints," *Applied Mathematical Modelling*, vol. 31, no. 5, pp. 895–911, 2007.
[17] J. S. Chen and H. H. Mo, "Numerical study on crack problems in segments of shield tunnel using finite element method," *Tunnelling and Underground Space Technology*, vol. 24, no. 1, pp. 91–102, 2009.
[18] D. S. Liyanapathirana and R. Nishanthan, "Influence of deep excavation induced ground movements on adjacent piles," *Tunnelling and Underground Space Technology*, vol. 52, pp. 168–181, 2016.
[19] M. P. Collins and D. Mitchell, *Prestressed Concrete Structures*, Prentice Hall, Englewood Cliffs, NJ, USA, 1991.
[20] GB 50010, *Code for Design of Concrete Structure*, China Architecture and Building Press, Beijing, China, 2010.
[21] H. Ma and D. Zhang, "Seismic response of a pre-stressed concrete wind turbine tower," *International Journal of Civil Engineering*, vol. 14, no. 9, pp. 561–571, 2016.
[22] H. Mashimo and T. Ishimura, "Evaluation of the load on shield tunnel lining in gravel," *Tunnelling and Underground Space Technology*, vol. 18, no. 2-3, pp. 233–241, 2003.
[23] G. X. Duan and H. Xu, "Analysis on stress observation results of full-scaled lining simulation model of tunnel crossing Yellow River," *Yangtze River*, vol. 42, no. 8, pp. 87–91, 2011.
[24] X. Q. Niu, Z. Y. Fu, and C. J. Zhang, "Full-scaled simulation model and experiment research on lining of tunnel crossing Yellow River," *Yangtze River*, vol. 42, no. 8, pp. 77–87, 2011.